

SC-wLS: Towards Interpretable Feed-forward Camera Re-localization

Xin Wu^{1,2*}, Hao Zhao^{1,3*}, Shunkai Li⁴, Yingdian Cao^{1,2}, and Hongbin Zha^{1,2}

¹ Key Laboratory of Machine Perception (MOE), School of AI, Peking University

² PKU-SenseTime Machine Vision Joint Lab

³ Intel Labs China

⁴ Kuaishou Technology

{wuxin1998,zhao-hao,lishunkai,yingdianc}@pku.edu.cn, zha@cis.pku.edu.cn

<https://github.com/XinWu98/SC-wLS>

Abstract. Visual re-localization aims to recover camera poses in a known environment, which is vital for applications like robotics or augmented reality. Feed-forward absolute camera pose regression methods directly output poses by a network, but suffer from low accuracy. Meanwhile, scene coordinate based methods are accurate, but need iterative RANSAC post-processing, which brings challenges to efficient end-to-end training and inference. In order to have the best of both worlds, we propose a feed-forward method termed SC-wLS that exploits all scene coordinate estimates for weighted least squares pose regression. This differentiable formulation exploits a weight network imposed on 2D-3D correspondences, and requires pose supervision only. Qualitative results demonstrate the interpretability of learned weights. Evaluations on 7Scenes and Cambridge datasets show significantly promoted performance when compared with former feed-forward counterparts. Moreover, our SC-wLS method enables a new capability: self-supervised test-time adaptation on the weight network. Codes and models are publicly available.

Keywords: Camera Re-localization, Differentiable Optimization

1 Introduction

Visual re-localization [10,16,32,38] determines the global 6-DoF poses (*i.e.*, position and orientation) of query RGB images in a known environment. It is a fundamental computer vision problem and has many applications in robotics and augmented reality. Recently there is a trend to incorporate deep neural networks into various 3D vision tasks, and use differentiable formulations that optimize losses of interest to learn result-oriented intermediate representation. Following this trend, many learning-based absolute pose regression (APR) methods [22,8] have been proposed for camera re-localization, which only need a single feed-forward pass to recover poses. However, they treat the neural network as a

* equal contribution

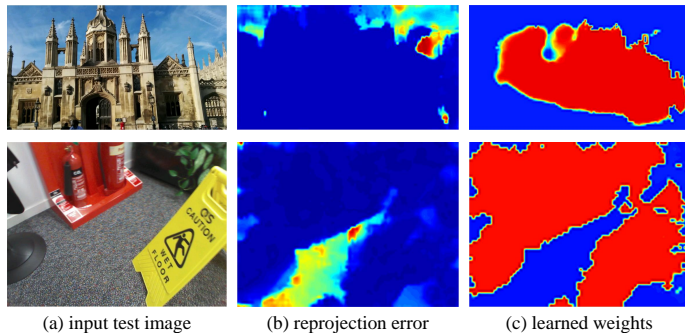


Fig. 1. For input images (a), our network firstly regresses their scene coordinates, then predicts correspondence-wise weights (c). With these weights, we can use all 2D-3D correspondences for end-to-end differentiable least squares pose estimation. We use re-projection errors (b) to illustrate scene coordinate quality. Our weights select high-quality scene coordinates. A higher color temperature represents a higher value.

black box and suffer from low accuracy [33]. On the other hand, scene coordinate based methods learn pixel-wise 3D scene coordinates from RGB images and solve camera poses using 2D-3D correspondences by Perspective-n-Point (PnP) [24]. In order to handle outliers in estimated scene coordinates, the random sample consensus (RANSAC) [11] algorithm is usually used for robust fitting. Compared to the feed-forward APR paradigm, scene coordinate based methods achieve state-of-the-art performance on public camera re-localization datasets. However, RANSAC-based post-processing is an iterative procedure conducted on CPUs, which brings engineering challenges for efficient end-to-end training and inference [4,7].

In order to get the best of both worlds, we develop a new feed-forward method based upon the state-of-the-art (SOTA) pipeline DSAC* [7], thus enjoying the strong representation power of scene coordinates. We propose an alternative option to RANSAC that exploits all 3D scene coordinate estimates for weighted least squares pose regression (SC-wLS). The key to SC-wLS is a weight network that treats 2D-3D correspondences as 5D point clouds and learns weights that capture geometric patterns in this 5D space, with only pose supervision. Our learned weights can be used to interpret how much each scene coordinate contributes to the least squares solver.

Our SC-wLS estimates poses using only tensor operators on GPUs, which is similar to APR methods due to the feed-forward nature but out-performs APR methods due to the usage of scene coordinates. Furthermore, we show that a self-supervised test-time adaptation step that updates the weight network can lead to further performance improvements. This is potentially useful in scenarios like a robot vacuum adapts to specific rooms during standby time. Although we focus on comparisons with APR methods, we also equip SC-wLS with the LM-Refine

post-processing module provided in DSAC* [7] to explore the limits of SC-wLS, and show that it out-performs SOTA on the outdoor dataset Cambridge.

Our major contributions can be summarized as follows: (1) We propose a new feed-forward camera re-localization method, termed SC-wLS, that learns interpretable scene coordinate quality weights (as in Fig. 1) for weighted least squares pose estimation, with only pose supervision. (2) Our method combines the advantages of two paradigms. It exploits learnt 2D-3D correspondences while still allows efficient end-to-end training and feed-forward inference in a principled manner. As a result, we achieve significantly better results than APR methods. (3) Our SC-wLS formulation allows test-time adaptation via self-supervised fine-tuning of the weight network with the photometric loss.

2 Related works

Camera re-localization. In the following, we discuss camera re-localization methods from the perspective of map representation.

Representing image databases with global descriptors like thumbnails [16], BoW [39], or learned features [1] is a natural choice for camera re-localization. By retrieving poses of similar images, localization can be done in the extremely large scale [16,34]. Meanwhile, CNN-based absolute pose regression methods [22,42,8,49] belong to this category, since their final-layer embeddings are also learned global descriptors. They regress camera poses from single images in an end-to-end manner, and recent work primarily focuses on sequential inputs [48] and network structure enhancement [49,37,13]. Although the accuracies of this line of methods are generally low due to intrinsic limitations [33], they are usually compact and fast, enabling pose estimation in a single feed-forward pass.

Maps can also be represented by 3D point cloud [46] with associated 2D descriptors [26] via SfM tools [35]. Given a query image, feature matching establishes sparse 2D-3D correspondences and yields very accurate camera poses with RANSAC-PnP pose optimization [53,32]. The success of these methods heavily depends on the discriminativeness of features and the robustness of matching strategies. Inspired by feature based pipelines, scene coordinate regression learns a 2D-3D correspondence for each pixel, instead of using feature extraction and matching separately. The map is implicitly encoded into network parameters. [27] demonstrates impressive localization performance using stereo initialization and sequence input. Recently, [2] shows that the algorithm used to create pseudo ground truth has a significant impact on the relative ranking of above methods.

Apart from random forest based methods using RGB-D inputs [38,40,28], scene coordinate regression on RGB images is seeing steady progress [4,5,6,7,56]. This line of work lays the foundation for our research. In this scheme, predicted scene coordinates are noisy due to single-view ambiguity and domain gap during inference. As such, [4,5] use RANSAC and non-linear optimization to deal with outliers, and NG-RANSAC [6] learns correspondence-wise weights to guide RANSAC sampling. [6] conditions weights on RGB images, whose statistics is often influenced by factors like lighting, weather or even exposure time. Object

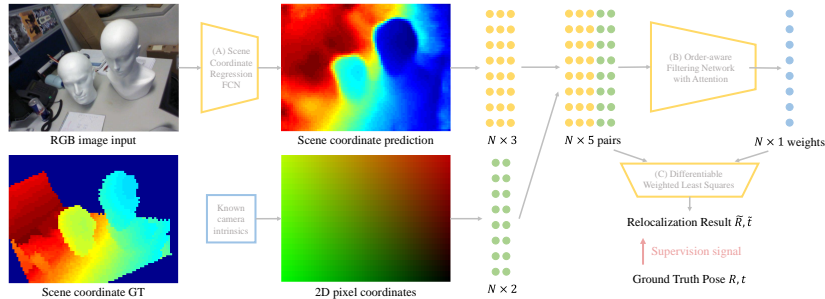


Fig. 2. The overview of SC-wLS. Firstly, a fully convolutional network (A) regresses pixel-wise scene coordinates from an input RGB image. Scene coordinate predictions are flattened to the shape of $N \times 3$, with N being pixel count. We concatenate it with normalized $N \times 2$ 2D pixel coordinates, forming $N \times 5$ correspondence inputs. The correspondences are fed into the weight learning network (B), producing $N \times 1$ weights indicating scene coordinate quality. The architecture of B is an order-aware filtering network [52] with graph attention modules [31]. Thirdly, correspondences and weights are sent into a differentiable weighted least squares layer (C), directly outputting camera poses. The scene coordinate ground truth is not used during training.

pose and room layout estimation [23,55,17,18,54,50] can also be addressed with similar representations [3,44].

Differentiable optimization. To enhance their compatibility with deep neural networks and learn result-oriented feature representation, some recent works focus on re-formulating geometric optimization techniques into an end-to-end trainable fashion, for various 3D vision tasks. [20] proposes several standard differentiable optimization layers. [51,30] propose to estimate fundamental/essential matrix via solving weighted least squares problems with spectral layers. [12] further shows that the eigen-value switching problem when solving least squares can be avoided by minimizing linear system residuals. [14] develops generic black-box differentiable optimization techniques with implicit declarative nodes.

3 Method

Given an RGB image I , we aim to find an estimate of the absolute camera pose consisting of a 3D translation and a 3D rotation, in the world coordinate system. Towards this goal, we exploit the scene coordinate representation. Specifically, for each pixel i with position \mathbf{p}_i in an image, we predict the corresponding 3D scene coordinate \mathbf{s}_i . As illustrated in Fig. 2, we propose an end-to-end trainable deep network that directly calculates global camera poses via weighted least squares. The method is named as **SC-wLS**. Fig. 2-A is a standard fully convolutional network for scene coordinate regression, as used in former works [7]. Our innovation lies in Fig. 2-B/C, as elaborated below.

3.1 Formulation

Given learned 3D scene coordinates and corresponding 2D pixel positions, our goal is to determine the absolute poses of calibrated images taking all correspondences into account. This would inevitably include outliers, and we need to give them proper weights. Ideally, if all outliers are rejected by zero weights, calculating the absolute pose can be formulated as a linear least squares problem. Inspired by [51] (which solves an essential matrix problem instead), we use all of the N 2D-3D correspondences as input and predict N respective weights \mathbf{w}_i using a neural network (Fig. 2-B). \mathbf{w}_i indicates the uncertainty of each scene coordinate prediction. As such the ideal least squares problem is turned into a weighted version for pose recovery.

Specifically, the input correspondence \mathbf{c}_i to Fig. 2-B is

$$\mathbf{c}_i = [x_i, y_i, z_i, u_i, v_i] \quad (1)$$

where x_i, y_i, z_i are the three components of the scene coordinate \mathbf{s}_i , and u_i, v_i denote the corresponding pixel position. u_i, v_i are generated by normalizing \mathbf{p}_i with the known camera intrinsic matrix. The absolute pose is written as a transformation matrix $\mathbf{T} \in \mathbb{R}^{3 \times 4}$. It projects scene coordinates to the camera plane as below:

$$\begin{bmatrix} u_i \\ v_i \\ 1 \end{bmatrix} = \mathbf{T} \begin{bmatrix} x_i \\ y_i \\ z_i \\ 1 \end{bmatrix} = \begin{bmatrix} p_1 & p_2 & p_3 & p_4 \\ p_5 & p_6 & p_7 & p_8 \\ p_9 & p_{10} & p_{11} & p_{12} \end{bmatrix} \begin{bmatrix} x_i \\ y_i \\ z_i \\ 1 \end{bmatrix} \quad (2)$$

When $N > 6$, the transformation matrix \mathbf{T} can be recovered by Direct Linear Transform (DLT) [15], which converts Eq. 2 into a linear system:

$$\mathbf{X} \text{Vec}(\mathbf{T}) = 0 \quad (3)$$

$\text{Vec}(\mathbf{T})$ is the vectorized \mathbf{T} . \mathbf{X} is a $\mathbb{R}^{2N \times 12}$ matrix whose $2i - 1$ and $2i$ rows $\mathbf{X}^{(2i-1)}$, $\mathbf{X}^{(2i)}$ are as follows:

$$\begin{bmatrix} x_i, y_i, z_i, 1, 0, 0, 0, 0, -u_i x_i, -u_i y_i, -u_i z_i, -u_i \\ 0, 0, 0, 0, x_i, y_i, z_i, 1, -v_i x_i, -v_i y_i, -v_i z_i, -v_i \end{bmatrix} \quad (4)$$

As such, pose estimation is formulated as a least squares problem. $\text{Vec}(\mathbf{T})$ can be recovered by finding the eigenvector associated to the smallest eigenvalue of $\mathbf{X}^\top \mathbf{X}$.

Note that in SC-wLS, each correspondence contributes differently according to \mathbf{w}_i , so $\mathbf{X}^\top \mathbf{X}$ can be rewritten as $\mathbf{X}^\top \text{diag}(\mathbf{w}) \mathbf{X}$ and $\text{Vec}(\mathbf{T})$ still corresponds to its smallest eigenvector. As the rotation matrix \mathbf{R} needs to be orthogonal and has determinant 1, we further refine the DLT results by the generalized Procrustes algorithm [36], which is also differentiable. More details about this post-processing step can be found in the supplementary material.

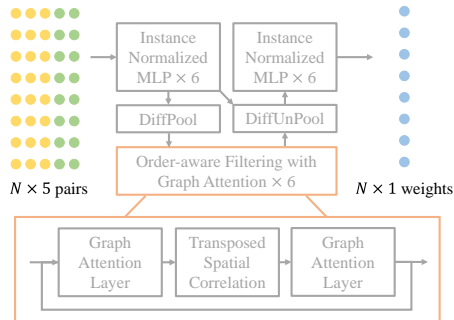


Fig. 3. The architecture of Fig. 2-B, which is inherited from OANet [52]. Here we use two self-attention graph layers from [31] while in the original OANet they are instance normalized MLPs.

3.2 Network design

Then we describe the architecture of Fig. 2-B. We treat the set of correspondences $\{c_i\}$ as unordered 5-dimensional point clouds and resort to a PointNet-like architecture [52] dubbed OANet. This hierarchical network design consists of multiple components including DiffPool layers, Order-Aware filtering blocks and DiffUnpool layers. It can guarantee the permutation-invariant property of input correspondences. Our improved version enhances the Order-Aware filtering block with self-attention.

The network is illustrated in Fig. 3. Specifically speaking, the DiffPool layer firstly clusters inputs into a particularly learned canonical order. Then the clusters are spatially correlated to retrieve the permutation-invariant context and finally recovered back to original size through the DiffUnpool operator. Inspired by the success of transformer [41] and its extension in 3D vision [31], we propose to introduce the self-attention mechanism into OANet to better reason about the underlying relationship between correspondences. As shown in Fig. 3, there are two instance normalized MLP modules before and after the transposed spatial correlation module, in original OANet. We replace them with attention-based message passing modules, which can exploit the spatial and contextual information simultaneously.

The clusters can be regarded as nodes $\mathcal{V} = \{v_i\}$ in a graph \mathcal{G} and the edges $\mathcal{E} = \{e_i\}$ are constructed between every two nodes. Since the number of clusters is significantly less than that of original inputs, calculating self-attention on these fully connected weighted edges would be tractable, in terms of computation speed and memory usage. Let ${}^{(\text{in})}\mathbf{f}_i$ be the intermediate representation for node v_i at input, and the self-attention operator can be described as:

$${}^{(\text{out})}\mathbf{f}_i = {}^{(\text{in})}\mathbf{f}_i + \text{MLP} \left(\left[\begin{array}{c} {}^{(\text{in})}\mathbf{f}_i \\ \mathbf{m}_{\mathcal{E} \rightarrow i} \end{array} \right] \right), \quad (5)$$

where $\mathbf{m}_{\mathcal{E} \rightarrow i}$ is the message aggregated from all other nodes $\{j : (i, j) \in \mathcal{E}\}$ using self-attention described in [31], and $[\cdot \parallel \cdot]$ denotes concatenation.

Finally, we apply two sequential activation functions (a ReLU followed by a Tanh) upon the outputs of Fig. 3 to get the weights \mathbf{w}_i in the range $[0, 1)$, for indoor scenes. We use the log-sigmoid activation for outdoor environments following [6], for more stable gradient back-propagation.

3.3 Loss functions

Generating ground-truth scene coordinates for supervision is time-consuming for real-world applications. To this end, our whole framework is solely supervised by ground-truth poses without accessing any 3D models. Successfully training the network with only pose supervision requires three stages using different loss functions. Before describing the training protocol, we first define losses here.

Re-projection loss is defined as follows:

$$r_i = \|\mathbf{K}\mathbf{T}^{-1}\mathbf{s}_i - \mathbf{p}_i\|_2, \quad (6)$$

$$\mathcal{L}_p^{(i)} = \begin{cases} r_i & \text{if } \mathbf{s}_i \in \mathbf{V} \\ \|\bar{\mathbf{s}}_i - \mathbf{s}_i\|_1 & \text{otherwise.} \end{cases} \quad (7)$$

$$\mathcal{L}_p = \frac{1}{N} \sum_{i=1}^N \mathcal{L}_p^{(i)} \quad (8)$$

\mathbf{K} is the known camera intrinsic matrix, and \mathbf{V} is a set of predicted \mathbf{s}_i that meet some specific validity constraints following DSAC* [7]. If $\mathbf{s}_i \in \mathbf{V}$, we use the re-projection error r_i in Eq. 6. Otherwise, we generate a heuristic $\bar{\mathbf{s}}_i$ assuming a depth of 10 meters. This hyper-parameter is inherited from [7].

Classification loss \mathcal{L}_c Without knowing the ground truth for scene coordinate quality weights, we utilize the re-projection error r_i for weak supervision:

$$l_i = \begin{cases} 0, & \text{if } r_i > \tau \\ 1, & \text{otherwise} \end{cases} \quad (9)$$

$$\mathcal{L}_c = \frac{1}{N} \sum_{i=1}^N H(l_i, \mathbf{w}_i), \quad (10)$$

where H is the binary cross-entropy function. τ is empirically set to 1 pixel to reject outliers. Ablation studies about \mathcal{L}_c can be found in the supplementary.

Regression loss \mathcal{L}_r Since our SC-wLS method is fully differentiable using the eigen-decomposition (ED) technique [20], imposing L_2 or other losses on the transform matrix \mathbf{T} is straightforward. However, as illustrated in [12], the eigen-decomposition operations would result in gradient instabilities due to the eigen vector switching phenomenon. Thus we utilize the eigen-decomposition free loss [12] to constrain the pose output, which avoids explicitly performing ED so as to guarantee convergence:

$$\mathcal{L}_r = \mathbf{t}^\top \mathbf{X}^\top \text{diag}(\mathbf{w}) \mathbf{X} \mathbf{t} + \alpha e^{-\beta \text{tr}(\bar{\mathbf{X}}^\top \text{diag}(\mathbf{w}) \bar{\mathbf{X}})} \quad (11)$$

where \mathbf{t} is the flattened ground-truth pose, $\bar{\mathbf{X}} = \mathbf{X}(\mathbf{I} - \mathbf{t}\mathbf{t}^\top)$, α and β are positive scalars. Two terms in Eq. 11 serve as different roles. The former tends to minimize the error of pose estimation while the latter tries to alleviate the impact of null space. The trace value in the second term can change up to thousands for different batches, thus the hyper-parameter β should be set to balance this effect.

3.4 Training protocol

We propose a three-stage protocol with different objective functions to train our network Fig. 2. Note that ground truth poses are known in all three stages.

Scene coordinate initialization. Firstly, we train our scene coordinate regression network (Fig. 2-A) by optimizing the re-projection error \mathcal{L}_p in Eq. 8, using ground truth poses. This step gives us reasonable initial scene coordinates, which are critical for the convergence of \mathcal{L}_c and \mathcal{L}_r .

Weight initialization. Secondly, we exploit $\mathcal{L} = \mathcal{L}_c + \gamma\mathcal{L}_r$ to train Fig. 2-B, where γ is a balancing weight. The classification loss \mathcal{L}_c is used to reject outliers. The regression loss \mathcal{L}_r is used to constrain poses, making a compromise between the accuracy of estimated weights and how much information is reserved in the null-space. \mathcal{L}_c is important to the stable convergence of this stage.

End-to-end optimization. As mentioned above, our whole pipeline is fully differentiable thus capable of learning both scene coordinates and quality weights, directly from ground truth poses. In the third stage, we train both the scene coordinate network (Fig. 2-A) and quality weight network (Fig. 2-B) using \mathcal{L} , forcing both of them to learn task-oriented feature representations.

3.5 Optional RANSAC-like post-processing

The SC-wLS method allows us to directly calculate camera poses with DLT. Although we focus on feed-forward settings, it is still possible to use RANSAC-like post-processing for better results. Specifically, we adopt the Levenberg-Marquardt solver developed by [7] to post-process DLT poses as an optional step (shortened as **LM-Refine**). It brings a boost of localization accuracy.

Specifically, this LM-Refine module is an iterative procedure. It first determines a set of inlier correspondences according to current pose estimate then optimizes poses using the Levenberg-Marquardt algorithm over the inlier set w.r.t. re-projection errors in Eq. 6. This process stops when the number of inlier set converges or until the maximum iteration, which we set to 100 following [7].

3.6 Self-supervised adaptation

At test time, we do not have ground truth pose for supervision. However, if the test data is given in the form of image sequences, we could use the photometric loss in co-visible RGB images to supervise our quality weight network Fig. 2-B. We sample two consecutive images I^s and I^t from the test set and synthesize \tilde{I}^t by warping I^s to I^t , similar to self-supervised visual odometry methods [57,25]:

$$p^t \sim \mathbf{K}\mathbf{T}_t^{-1}\mathbf{s}^s \quad (12)$$

Table 1. Median errors on the 7Scenes dataset [38], with translational and rotational errors measured in m and $^\circ$. Our results are evaluated directly using weighted DLT, without the (optional) LM-Refine step (Section 3.5) and self-supervised adaptation step (Section 3.6). We compare with methods that directly predict poses with neural networks. Ours (dlt) and Ours ($dlt+e2e$) show results evaluated w/o and w/ the third stage mentioned in Section 3.4. Our results are significantly better.

Methods	Chess	Fire	Heads	Office	Pumpkin	Kitchen	Stairs
PoseNet17 [21]	0.13/4.5	0.27/11.3	0.17/13.0	0.19/5.6	0.26/4.8	0.23/5.4	0.35/12.4
LSTM-Pose [42]	0.24/5.8	0.34/11.9	0.21/13.7	0.30/8.1	0.33/7.0	0.37/8.8	0.40/13.7
BranchNet [47]	0.18/5.2	0.34/9.0	0.20/14.2	0.30/7.1	0.27/5.1	0.33/7.4	0.38/10.3
GPoseNet [9]	0.20/7.1	0.38/12.3	0.21/13.8	0.28/8.8	0.37/6.9	0.35/8.2	0.37/12.5
MLFBPPose [45]	0.12/5.8	0.26/12.0	0.14/13.5	0.18/8.2	0.21/7.1	0.22/8.1	0.38/10.3
AttLoc [43]	0.10/4.1	0.25/11.4	0.16/11.8	0.17/5.3	0.21/4.4	0.23/5.4	0.26/10.5
MapNet [8]	0.08/3.3	0.27/11.7	0.18/13.3	0.17/5.2	0.22/4.0	0.23/4.9	0.30/12.1
LsG [48]	0.09/3.3	0.26/10.9	0.17/12.7	0.18/5.5	0.20/3.7	0.23/4.9	0.23/11.3
GL-Net [49]	0.08/2.8	0.26/8.9	0.17/11.4	0.18/5.1	0.15/2.8	0.25/4.5	0.23/8.8
MS-Transformer [37]	0.11/4.7	0.24/9.6	0.14/12.2	0.17/5.7	0.18/4.4	0.17/5.9	0.26/8.5
Ours (dlt)	0.029/0.78	0.051/1.04	0.026 /2.00	0.063/0.93	0.084/1.28	0.099/1.60	0.179/3.61
Ours ($dlt+e2e$)	0.029 /0.76	0.048 /1.09	0.027/ 1.92	0.055 /0.86	0.077 /1.27	0.091 /1.43	0.123 /2.80

$$\mathcal{L}_{\text{ph}} = \sum_p \|\tilde{I}^t(p) - \tilde{I}^s(p)\|_1 + \mathcal{L}_{\text{SSIM}} \quad (13)$$

where p indexes over pixel coordinates, and \tilde{I}^t is the source view I^s warped to the target frame based on the predicted global scene coordinates \mathbf{s}^s . $\mathcal{L}_{\text{SSIM}}$ is the structured similarity loss [58] imposed on $\tilde{I}^t(p)$ and $\tilde{I}^s(p)$.

Scene coordinates can be trained by \mathcal{L}_{ph} via two gradient paths: (1) the sampling location generation process in Eq. 12. (2) the absolute pose \mathbf{T}_t which is calculated by DLT on scene coordinates. However, we observe that fine-tuning scene coordinates with \mathcal{L}_{ph} results in divergence. To this end, we detach scene coordinates from computation graphs and only fine-tune the quality weight net (Fig. 2-B) with self supervision. As will be shown later in experiments, this practice greatly improves re-localization performance. A detailed illustration of this adaptation scheme is provided in the supplementary material.

To clarity, our test-time adaptation experiments exploit all frames in the test set for self-supervision. An ideal online formulation would only use frames before the one of interest. The current offline version can be useful in scenarios like robot vacuums adapts to specific rooms during standby time.

4 Experiments

4.1 Experiment setting

Datasets. We evaluate our SC-wLS framework for camera re-localization from single RGB images, on both indoor and outdoor scenes. Following [7], we choose the publicly available indoor 7Scenes dataset [38] and outdoor Cambridge dataset [22], which have different scales, appearance and motion patterns. These two

Table 2. Median errors on the Cambridge dataset [22], with translational and rotational errors measured in m and $^\circ$. Settings are the same as Table 1. Our results are significantly better than other methods. Note that GL-Net uses a sequence as input.

Methods	Greatcourt	King’s College	Shop Facade	Old Hospital	Church
ADPoseNet [19]	N/A	1.30/1.7	1.22/6.7	N/A	2.28/4.8
PoseNet17 [21]	7.00/3.7	0.99/1.1	1.05/4.0	2.17/2.9	1.49/3.4
GPoseNet [9]	N/A	1.61/2.3	1.14/5.7	2.62/3.9	2.93/6.5
MLFBPPose [45]	N/A	0.76/1.7	0.75/5.1	1.99/2.9	1.29/5.0
LSTM-Pose [42]	N/A	0.99/3.7	1.18/7.4	1.51/4.3	1.52/6.7
SVS-Pose [29]	N/A	1.06/2.8	0.63/5.7	1.50/4.0	2.11/8.1
MapNet [8]	N/A	1.07/1.9	1.49/4.2	1.94/3.9	2.00/4.5
GL-Net [49]	6.67/2.8	0.59/0.7	0.50/2.9	1.88/2.8	1.90/3.3
MS-Transformer [37]	N/A	0.83/1.5	0.86/3.1	1.81/2.4	1.62/4.0
Ours (<i>dlt</i>)	1.81/1.2	0.22/0.9	0.15/1.1	0.46/1.9	0.50/1.5
Ours (<i>dlt+e2e</i>)	1.64/0.9	0.14/0.6	0.11/0.7	0.42/1.7	0.39/1.3

datasets have fairly different distributions of scene coordinates. We would show later that, in both cases, SC-wLS successfully predicts interpretable scene coordinate weights for feed-forward camera re-localization.

Implementation. The input images are proportionally resized so that the heights are 480 pixels. We randomly zoom and rotate images for data augmentation following [7]. As mentioned in Sec. 3.3, α and β in Eq. 11 are sensitive to specific scenes. We set them to 5 and $1e-4$ for indoor 7Scenes while 5 and $1e-6$ for outdoor Cambridge, respectively. The balancing hyper-parameter γ is set to 5 empirically. We train our model on one nVIDIA GeForce RTX 3090 GPU. The ADAM optimizer with initial learning rate $1e-4$ is utilized in the first two training stages and the learning rate is set to $1e-5$ in the end-to-end training stage. The batch size is set to 1 as [7]. The scene coordinate regression network architecture for 7Scenes is adopted from [7]. As for Cambridge, we add residual connections to the early layers of this network. Architecture details can be found in the supplementary material.

4.2 Feed-forward Re-localization

An intriguing property of the proposed SC-wLS method is that we can re-localize a camera directly using weighted least squares. This inference scheme seamlessly blends into the forward pass of a neural network. So we firstly compare with other APR re-localization methods that predict camera poses directly with a neural network during inference. Quantitative results on 7Scenes and Cambridge are summarized in Table 1 and Table 2, respectively.

As for former arts, we distinguish between two cases: single frame based and sequence based. They are separated by a line in Table 1 and Table 2. As for our results, we report under two settings: Ours (*dlt*) and Ours (*dlt+e2e*). Ours (*dlt+e2e*) means all three training stages are finished (see Section 3.4), while Ours (*dlt*) means only the first two stages are used.

Table 3. Results on the 7Scenes dataset [38] and the Cambridge dataset [22], with translational and rotational errors measured in m and $^\circ$. Here *ref* means LM-Refine. Note DSAC* [7] w/o model and NG-RANSAC [6] also use the LM pose refinement process. Note that with *ref* used, our method loses the feed-forward nature. NG-RANSAC w/o model† is retrained using DSAC* RGB initialization.

7Scenes	Chess	Fire	Heads	Office	Pumpkin	Kitchen	Stairs
DSAC* [7] w/o model	0.019/1.11	0.019 /1.24	0.011 /1.82	0.026 /1.18	0.042 /1.42	0.030 /1.70	0.041 /1.42
Ours (<i>dlt+ref</i>)	0.018 /0.63	0.026/ 0.84	0.015/ 0.87	0.038/0.85	0.045/ 1.05	0.051/1.17	0.067/1.93
Ours (<i>dlt+e2e+ref</i>)	0.019/ 0.62	0.025/0.88	0.014/0.90	0.035/ 0.78	0.051/1.07	0.054/ 1.15	0.058/1.57
Cambridge	Greatcourt	King's College	Shop Facade	Old Hospital	Church		
DSAC* [7] w/o model	0.34/0.2	0.18/0.3	0.05/1.3	0.21/0.4	0.15/0.6		
NG-RANSAC [6]	0.35/0.2	0.13/0.2	0.06/0.3	0.22/0.4	0.10/0.3		
NG-RANSAC w/o model†	0.31/0.2	0.15/0.3	0.05/0.3	0.20/0.4	0.12/0.4		
Ours (<i>dlt+ref</i>)	0.32/0.2	0.09/0.3	0.04/0.3	0.12/0.4	0.12/0.4		
Ours (<i>dlt+e2e+ref</i>)	0.29 / 0.2	0.08 / 0.2	0.04 / 0.3	0.11 / 0.4	0.09 / 0.3		

Table 4. Recalls (%) on the 7Scenes dataset [38] and the Cambridge dataset [22].

7Scenes	Chess	Fire	Heads	Office	Pumpkin	Kitchen	Stairs	Avg
DSAC* [7] w/o model	96.7	92.9	98.2	87.1	60.7	65.3	64.1	80.7
Active Search [32]	86.4	86.3	95.7	65.6	34.1	45.1	67.8	68.7
Ours (<i>dlt+e2e+ref</i>)	93.7	82.2	65.7	73.5	49.6	45.3	43.0	64.7
Ours (<i>dlt+e2e+dsac*</i>)	96.8	97.4	94.3	88.6	62.4	65.5	55.3	80.0
Cambridge	Great Court	King's College	Shop Facade	Old Hospital	Church	Avg		
DSAC* [7] w/o model	62.9	80.8	86.4	55.5	88.9	74.9		
NG-RANSAC w/o model†	67.6	81.9	88.3	56.0	93.8	77.5		
Ours (<i>dlt+e2e+ref</i>)	73.3	97.3	90.3	75.3	82.2	83.7		
Ours (<i>dlt+e2e+dsac*</i>)	74.3	87.2	87.4	53.8	99.1	80.4		

On 7Scenes, it is clear that our SC-wLS method out-performs APR camera re-localization methods by significant margins. Note we only take a single image as input, and still achieve much lower errors than sequence-based methods like GLNet [49]. On Cambridge, SC-wLS also reports significantly better results including the Greatcourt scene. Note that this scene has extreme illumination conditions and most former solutions do not even work.

Why SC-wLS performs much better than former APR methods that directly predict poses without RANSAC? Because they are black boxes, failing to model explicit geometric relationships. These black-box methods suffer from hard memorization and dataset bias. By contrast, our formulation is based upon 2D-3D correspondences, while still allowing feed-forward inference.

Lastly, Ours (*dlt+e2e*) shows lower errors than Ours (*dlt*) in most scenes, validating the effectiveness of jointly fine-tuning Fig. 2-A and Fig. 2-B.

4.3 Optional LM-Refine

The most interesting part about SC-wLS is the strong re-localization ability without using iterative pose estimation methods like RANSAC or LM-Refine.

Table 5. Results on the 7Scenes dataset [38] and the Cambridge dataset [22], with translational and rotational errors measured in m and $^\circ$. Here *self* means self-supervised adaptation. Note these results are evaluated without LM-Refine.

7Scenes	Chess	Fire	Heads	Office	Pumpkin	Kitchen	Stairs
Ours (<i>dlt+e2e</i>)	0.029/0.76	0.048/1.09	0.027/1.92	0.055/0.86	0.077/1.27	0.091/1.43	0.123/2.80
Ours (<i>dlt+e2e+self</i>)	0.021/0.64	0.023/0.80	0.013/0.79	0.037/0.76	0.048/1.06	0.051/1.08	0.055/1.48
Cambridge	Greatcourt	King's College	Shop Facade	Old Hospital	Church		
Ours (<i>dlt+e2e</i>)	1.64/0.9	0.14/0.6	0.11/0.7	0.42/1.7	0.39/1.3		
Ours (<i>dlt+e2e+self</i>)	0.94/0.5	0.11/0.3	0.05/0.4	0.18/0.7	0.17/0.8		

However, although optional, incorporating such methods does lead to lower errors. We report quantitative comparisons in Table 3. We compare with the best published method DSAC* in the 'w/o model' setting for two reasons: 1) Our training protocol does not involve any usage of 3D models; 2) DSAC* also uses LM-Refine as a post-processing step. Note LM-Refine needs pose initialization, so we use DLT results as initial poses. Similar to above experiments, Ours (*dlt+e2e+ref*) means all three training stages are used. For Cambridge, we also compare to NG-RANSAC [6], which predicts weights from RGB images.

On the Cambridge dataset, SC-wLS outperforms state-of-the-art methods. On the Old Hospital scene, we reduce the translational error from 0.21m to 0.11m, which is a 47.6% improvement. Meanwhile, Ours (*dlt+e2e+ref*) consistently achieves lower errors than Ours (*dlt+ref*), showing the benefits of end-to-end joint learning. On the 7Scenes dataset, our results under-perform DSAC* and the third training stage does not bring clear margins.

We also report average recalls with pose error below 5cm, 5deg (7Scenes) and translation error below 0.5% of the scene size (Cambridge) in Table 4. It is demonstrated that the recall value of Ours (*dlt+e2e+ref*) under-performs SOTA on 7Scenes, which is consistent with the median error results. We also evaluate DSAC*'s exact post-processing, denoted as Our (*dlt+e2e+dsac**). The difference is that for Ours (*dlt+e2e+ref*) we use DLT results for LM-Refine initialization and for Ours (*dlt+e2e+dsac**) we use RANSAC for LM-Refine initialization. It is shown that using DSAC*'s exact post-processing can compensate for the performance gap on 7Scenes.

4.4 Self-supervised Adaptation

We show the effectiveness of self-supervised weight network adaptation during test time, which is a potentially useful new feature of SC-wLS (Section 3.6). Results are summarized in Table 5, which is evaluated under the weighted DLT setting (same as Section 4.2). Obviously, for all sequences in 7Scenes and Cambridge, Ours (*dlt+e2e+self*) outperforms Ours (*dlt+e2e*) by clear margins. On *Stairs* and *Old Hospital*, translational and rotational error reductions are both over 50%. In these experiments, self-supervised adaptation runs for about 600k iterations. Usually, this adaptation process converges to a reasonably good state, within only 150k iterations. More detailed experiments are in the supplementary.

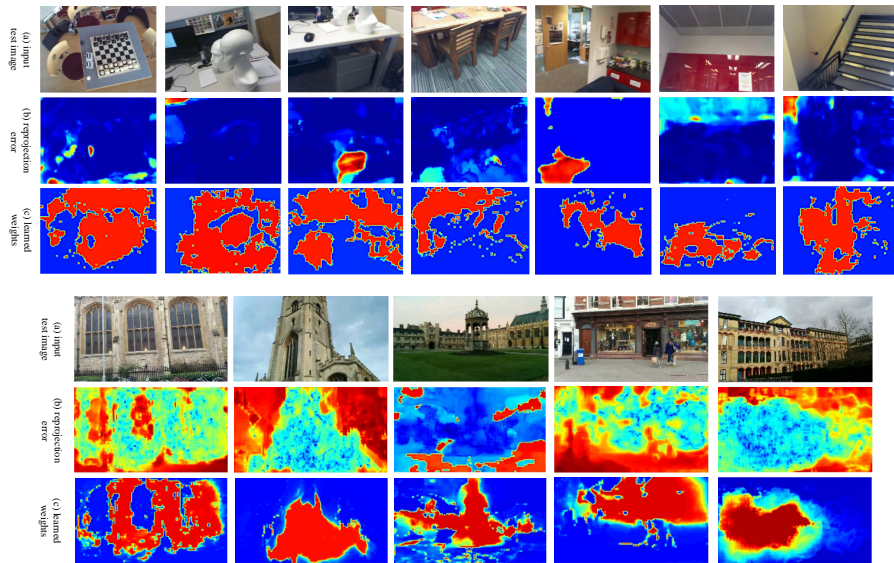


Fig. 4. Visualizations on 7Scenes and Cambridge test sets, demonstrating that our network learns interpretable scene coordinate weights consistent with re-projection errors, by solely considering the intrinsic structure of input 2D-3D correspondences. A higher color temperature represents a higher value.

4.5 Visualization

Firstly, we demonstrate more learnt weights on the test sets of 7Scenes and Cambridge, in Fig. 4. The heatmaps for reprojection error and learnt weight are highly correlated. Pixels with low quality weights usually have high reprojection errors and occur in sky or uniformly textured regions.

Secondly, We show learnt 3D maps with and without quality filtering, in Fig. 5. Since scene coordinates are predicted in the world frame, we directly show the point clouds generated by aggregating scene coordinate predictions on test frames. It is shown that only predicting scene coordinates results in noisy point clouds, especially in outdoor scenes where scene coordinate predictions on sky regions are only meaningful in term of their 2D projections. We show good scene coordinates by filtering out samples with a quality weight lower than 0.9.

4.6 Training and Inference Efficiency

As shown in Table 6, our method, as a feed-forward (*fw*) one, is faster than the well-engineered iterative (*iter*) method DSAC* and the transformer-based method MS-Transformer [37]. We could make a tradeoff using OANet w/o attention for even faster speed. Thus it’s reasonable to compare our feed-forward method with APR methods. We also evaluate end-to-end training efficiency.

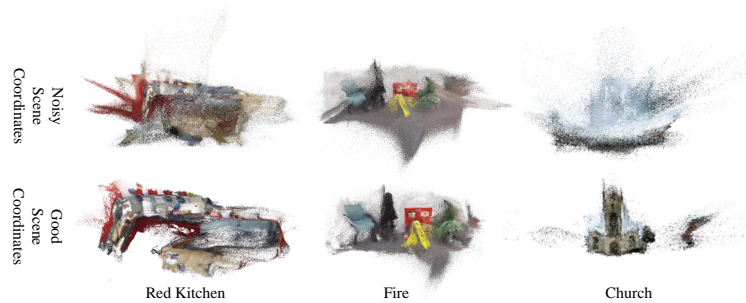


Fig. 5. Map visualization on 7Scenes and Cambridge. More comparisons are provided in the supplementary material.

Table 6. Average end-to-end training and inference time comparisons.

Method	Inference time (ms/frame)						End-to-end training time (s/frame)			
	AtLoc [43]	MapNet [8]	Ours (OANet)	Ours	MS-T [37]	DSAC* [7]	Setting	Ours	DSAC* [7]	NG-RANSAC [6]
Type	<i>fw</i>	<i>fw</i>	<i>fw</i>	<i>fw</i>	<i>fw</i>	<i>iter</i>	1-GPU	0.09	0.20	0.31
Time	6	9	13	19	30	32	5-GPU	0.09	0.85	1.05

When training 5 network instances for 5 different scenes on 5 GPUs, the average time of ours stays unchanged, while that of DSAC* increases due to limited CPU computation/scheduling capacity. We believe large-scale training of many re-localization network instances on the cloud is an industry demand.

5 Conclusions

In this study, we propose a new camera re-localization solution named SC-wLS, which combines the advantages of feed-forward formulations and scene coordinate based methods. It exploits the correspondences between pixel coordinates and learnt 3D scene coordinates, while still allows direct camera re-localization through a single forward pass. This is achieved by a correspondence weight network that finds high-quality scene coordinates, supervised by poses only. Meanwhile, SC-wLS also allows self-supervised test-time adaptation. Extensive evaluations on public benchmarks 7Scenes and Cambridge demonstrate the effectiveness and interpretability of our method. In the feed-forward setting, SC-wLS results are significantly better than APR methods. When coupled with LM-Refine post-processing, our method out-performs SOTA on outdoor scenes and under-performs SOTA on indoor scenes.

Acknowledgement This work was supported by the National Natural Science Foundation of China under Grant 62176010.

References

1. Arandjelovic, R., Gronat, P., Torii, A., Pajdla, T., Sivic, J.: Netvlad: Cnn architecture for weakly supervised place recognition. In: Proceedings of the IEEE conference on computer vision and pattern recognition. pp. 5297–5307 (2016) [3](#)
2. Brachmann, E., Humenberger, M., Rother, C., Sattler, T.: On the limits of pseudo ground truth in visual camera re-localisation. In: Proceedings of the IEEE/CVF International Conference on Computer Vision. pp. 6218–6228 (2021) [3](#)
3. Brachmann, E., Krull, A., Michel, F., Gumhold, S., Shotton, J., Rother, C.: Learning 6d object pose estimation using 3d object coordinates. In: European conference on computer vision. pp. 536–551. Springer (2014) [4](#)
4. Brachmann, E., Krull, A., Nowozin, S., Shotton, J., Michel, F., Gumhold, S., Rother, C.: Dsac-differentiable ransac for camera localization. In: CVPR (2017) [2, 3](#)
5. Brachmann, E., Rother, C.: Learning less is more - 6d camera localization via 3d surface regression. CVPR (2018) [3](#)
6. Brachmann, E., Rother, C.: Neural-guided ransac: Learning where to sample model hypotheses. ICCV (2019) [3, 7, 11, 12, 14](#)
7. Brachmann, E., Rother, C.: Visual camera re-localization from rgb and rgb-d images using dsac. IEEE Transactions on Pattern Analysis and Machine Intelligence (2021) [2, 3, 4, 7, 8, 9, 10, 11, 14](#)
8. Brahmabhatt, S., Gu, J., Kim, K., Hays, J., Kautz, J.: Geometry-aware learning of maps for camera localization. In: CVPR (2018) [1, 3, 9, 10, 14](#)
9. Cai, M., Shen, C., Reid, I.: A hybrid probabilistic model for camera relocalization (2019) [9, 10](#)
10. Cao, S., Snavely, N.: Graph-based discriminative learning for location recognition. In: IJCV (2015) [1](#)
11. Choi, S., Kim, T., Yu, W.: Performance evaluation of ransac family. Journal of Computer Vision **24**(3), 271–300 (1997) [2](#)
12. Dang, Z., Yi, K.M., Hu, Y., Wang, F., Fua, P., Salzmann, M.: Eigendecomposition-free training of deep networks for linear least-square problems. TPAMI (2020) [4, 7](#)
13. Ding, M., Wang, Z., Sun, J., Shi, J., Luo, P.: Camnet: Coarse-to-fine retrieval for camera re-localization. In: Proceedings of the IEEE/CVF International Conference on Computer Vision. pp. 2871–2880 (2019) [3](#)
14. Gould, S., Hartley, R., Campbell, D.J.: Deep declarative networks. TPAMI (2021) [4](#)
15. Hartley, R., Zisserman, A.: Multiple view geometry in computer vision: N-view geometry (2004) [5](#)
16. Hays, J., Efros, A.A.: Im2gps: estimating geographic information from a single image. In: CVPR (2008) [1, 3](#)
17. Hedau, V., Hoiem, D., Forsyth, D.: Recovering the spatial layout of cluttered rooms. In: 2009 IEEE 12th international conference on computer vision. pp. 1849–1856. IEEE (2009) [4](#)
18. Hirzer, M., Lepetit, V., ROTH, P.: Smart hypothesis generation for efficient and robust room layout estimation. In: Proceedings of the IEEE/CVF winter conference on applications of computer vision. pp. 2912–2920 (2020) [4](#)
19. Huang, Z., Xu, Y., Shi, J., Zhou, X., Bao, H., Zhang, G.: Prior guided dropout for robust visual localization in dynamic environments. In: ICCV (2019) [10](#)

20. Ionescu, C., Vantzos, O., Sminchisescu, C.: Matrix backpropagation for deep networks with structured layers. In: ICCV (2015) [4](#), [7](#)
21. Kendall, A., Cipolla, R.: Geometric loss functions for camera pose regression with deep learning. In: CVPR (2017) [9](#), [10](#)
22. Kendall, A., Grimes, M., Cipolla, R.: PoseNet: A convolutional network for real-time 6-dof camera relocalization. In: ICCV (2015) [1](#), [3](#), [9](#), [10](#), [11](#), [12](#)
23. Lepetit, V., Fua, P., et al.: Monocular model-based 3d tracking of rigid objects: A survey. *Foundations and Trends® in Computer Graphics and Vision* **1**(1), 1–89 (2005) [4](#)
24. Li, S., Xu, C., Xie, M.: A robust o(n) solution to the perspective-n-point problem. *IEEE transactions on pattern analysis and machine intelligence* **34**(7), 1444–1450 (2012) [2](#)
25. Li, S., Wu, X., Cao, Y., Zha, H.: Generalizing to the open world: Deep visual odometry with online adaptation. In: Proceedings of the IEEE/CVF Conference on Computer Vision and Pattern Recognition. pp. 13184–13193 (2021) [8](#)
26. Lowe, D.G.: Distinctive image features from scale-invariant keypoints. *IJCV* (2004) [3](#)
27. Mair, E., Strobl, K.H., Suppa, M., Burschka, D.: Efficient camera-based pose estimation for real-time applications. In: 2009 IEEE/RSJ International Conference on Intelligent Robots and Systems. pp. 2696–2703. IEEE (2009) [3](#)
28. Meng, L., Tung, F., Little, J.J., Valentin, J., de Silva, C.W.: Exploiting points and lines in regression forests for rgb-d camera relocalization. In: IROS (2018) [3](#)
29. Naseer, T., Burgard, W.: Deep regression for monocular camera-based 6-dof global localization in outdoor environments. In: IROS (2017) [10](#)
30. Ranftl, R., Koltun, V.: Deep fundamental matrix estimation. In: ECCV (2018) [4](#)
31. Sarlin, P.E., DeTone, D., Malisiewicz, T., Rabinovich, A.: Superglue: Learning feature matching with graph neural networks. In: CVPR (2020) [4](#), [6](#)
32. Sattler, T., Leibe, B., Kobbelt, L.: Efficient & effective prioritized matching for large-scale image-based localization. *TPAMI* (2016) [1](#), [3](#), [11](#)
33. Sattler, T., Zhou, Q., Pollefeys, M., Leal-Taixe, L.: Understanding the limitations of cnn-based absolute camera pose regression. In: CVPR (2019) [2](#), [3](#)
34. Schindler, G., Brown, M., Szeliski, R.: City-scale location recognition. In: CVPR (2007) [3](#)
35. Schonberger, J.L., Frahm, J.M.: Structure-from-motion revisited. In: Proceedings of the IEEE conference on computer vision and pattern recognition. pp. 4104–4113 (2016) [3](#)
36. Schönemann, P.H.: A generalized solution of the orthogonal procrustes problem. *Psychometrika* **31**(1), 1–10 (1966) [5](#)
37. Shavit, Y., Ferens, R., Keller, Y.: Learning multi-scene absolute pose regression with transformers. In: Proceedings of the IEEE/CVF International Conference on Computer Vision. pp. 2733–2742 (2021) [3](#), [9](#), [10](#), [13](#), [14](#)
38. Shotton, J., Glocker, B., Zach, C., Izadi, S., Criminisi, A., Fitzgibbon, A.: Scene coordinate regression forests for camera relocalization in rgb-d images. In: CVPR (2013) [1](#), [3](#), [9](#), [11](#), [12](#)
39. Sivic, J., Zisserman, A.: Video google: A text retrieval approach to object matching in videos. In: ICCV (2003) [3](#)
40. Valentin, J., Nießner, M., Shotton, J., Fitzgibbon, A., Izadi, S., Torr, P.H.: Exploiting uncertainty in regression forests for accurate camera relocalization. In: CVPR (2015) [3](#)
41. Vaswani, A., Shazeer, N., Parmar, N., Uszkoreit, J., Jones, L., Gomez, A.N., Kaiser, L., Polosukhin, I.: Attention is all you need (2017) [6](#)

42. Walch, F., Hazirbas, C., Leal-Taixe, L., Sattler, T., Hilsenbeck, S., Cremers, D.: Image-based localization using lstms for structured feature correlation. In: ICCV (2017) [3](#), [9](#), [10](#)
43. Wang, B., Chen, C., Lu, C.X., Zhao, P., Trigoni, N., Markham, A.: Atloc: Attention guided camera localization. In: Proceedings of the AAAI Conference on Artificial Intelligence. vol. 34, pp. 10393–10401 (2020) [9](#), [14](#)
44. Wang, H., Sridhar, S., Huang, J., Valentin, J., Song, S., Guibas, L.J.: Normalized object coordinate space for category-level 6d object pose and size estimation. In: Proceedings of the IEEE/CVF Conference on Computer Vision and Pattern Recognition. pp. 2642–2651 (2019) [4](#)
45. Wang, X., Wang, X., Wang, C., Bai, X., Wu, J., Hancock, E.R.: Discriminative features matter: Multi-layer bilinear pooling for camera localization. In: BMVC (2019) [9](#), [10](#)
46. Wu, C.: Towards linear-time incremental structure from motion. In: 3DV (2013) [3](#)
47. Wu, J., Ma, L., Hu, X.: Delving deeper into convolutional neural networks for camera relocalization. In: ICRA (2017) [9](#)
48. Xue, F., Wang, X., Yan, Z., Wang, Q., Wang, J., Zha, H.: Local supports global: Deep camera relocalization with sequence enhancement. In: ICCV (2019) [3](#), [9](#)
49. Xue, F., Wu, X., Cai, S., Wang, J.: Learning multi-view camera relocalization with graph neural networks. In: 2020 IEEE/CVF Conference on Computer Vision and Pattern Recognition (CVPR). pp. 11372–11381. IEEE (2020) [3](#), [9](#), [10](#), [11](#)
50. Yan, C., Shao, B., Zhao, H., Ning, R., Zhang, Y., Xu, F.: 3d room layout estimation from a single rgb image. IEEE Transactions on Multimedia **22**(11), 3014–3024 (2020) [4](#)
51. Yi, K., Trulls, E., Ono, Y., Lepetit, V., Salzmann, M., Fua, P.: Learning to find good correspondences. CVPR (2018) [4](#), [5](#)
52. Zhang, J., Sun, D., Luo, Z., Yao, A., Zhou, L., Shen, T., Chen, Y., Quan, L., Liao, H.: Learning two-view correspondences and geometry using order-aware network. In: ICCV (2019) [4](#), [6](#)
53. Zhang, W., Kosecka, J.: Image based localization in urban environments. In: 3DPTV (2006) [3](#)
54. Zhao, H., Lu, M., Yao, A., Guo, Y., Chen, Y., Zhang, L.: Physics inspired optimization on semantic transfer features: An alternative method for room layout estimation. In: Proceedings of the IEEE conference on computer vision and pattern recognition. pp. 10–18 (2017) [4](#)
55. Zhong, L., Zhang, Y., Zhao, H., Chang, A., Xiang, W., Zhang, S., Zhang, L.: Seeing through the occluders: Robust monocular 6-dof object pose tracking via model-guided video object segmentation. IEEE Robotics and Automation Letters **5**(4), 5159–5166 (2020) [4](#)
56. Zhou, L., Luo, Z., Shen, T., Zhang, J., Zhen, M., Yao, Y., Fang, T., Quan, L.: Kfnet: Learning temporal camera relocalization using kalman filtering. In: Proceedings of the IEEE/CVF Conference on Computer Vision and Pattern Recognition. pp. 4919–4928 (2020) [3](#)
57. Zhou, T., Brown, M., Snavely, N., Lowe, D.G.: Unsupervised learning of depth and ego-motion from video. In: CVPR (2017) [8](#)
58. Zhou Wang, Bovik, A.C., Sheikh, H.R., Simoncelli, E.P.: Image quality assessment: from error visibility to structural similarity. IEEE Transactions on Image Processing **13**(4), 600–612 (2004). <https://doi.org/10.1109/TIP.2003.819861> [9](#)

Supplementary Material of SC-wLS: Towards Interpretable Feed-forward Camera Re-localization

Xin Wu^{1,2*}, Hao Zhao^{1,3*}, Shunkai Li⁴, Yingdian Cao^{1,2}, and Hongbin Zha^{1,2}

¹ Key Laboratory of Machine Perception (MOE), School of EECS, Peking University

² PKU-SenseTime Machine Vision Joint Lab

³ Intel Labs China

⁴ Kuaishou Technology

{wuxin1998,zhao-hao,lishunkai,yingdianc}@pku.edu.cn, zha@cis.pku.edu.cn

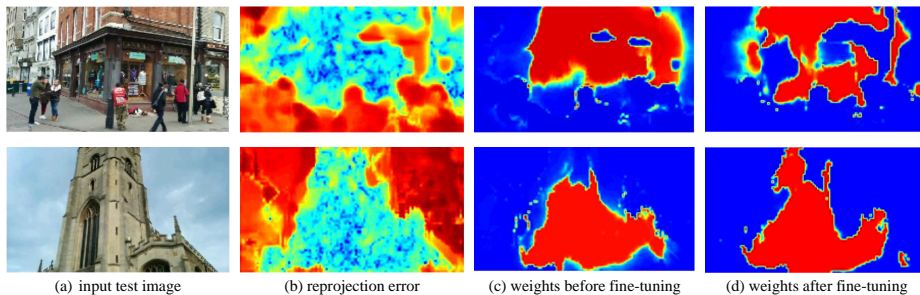


Fig. 1. After self-supervised fine-tuning during test time, the quality network selects better scene coordinates.

1 Evaluations with SfM ground truth on 7Scenes dataset

As illustrated in [1], the reference algorithm used to create pseudo ground truth has an influence on the performance of a certain family of re-localisation methods. Thus we also train (w/o 3D model) and evaluate our method using the pseudo ground truth (pGT) generated by SfM [1] on 7Scenes dataset. In Table 1, we report the median translational and rotational errors and recalls with pose error below 5cm, 5deg, and the settings are the same as Table 1, 4 in the main paper. Compared with the results on the original 7Scenes dataset, the performance of our methods trained with pGT-SfM improves on all of the scenes, which is consistent with other re-localization methods reported in [1]. Besides, it is shown that the recalls of our method Ours ($dlt+e2e+ref$) under-perform DSAC* (w/ model), and using DSAC*'s exact post-processing can compensate for this gap.

* equal contribution

Table 1. Results on the 7Scenes dataset [6], with translational and rotational errors measured in m and $^\circ$, and recalls (%) with pose error below $5cm$, 5° . Here notations are the same as the Table 1, 4 in the main paper. Note DSAC* [1] w/ model is trained with 3D model, and all of these methods are trained using pseudo ground truth generated by SfM [1].

Median Errors	Chess	Fire	Heads	Office	Pumpkin	Kitchen	Stairs	
Ours (dlt)	0.012/0.39	0.030/0.59	0.024/1.53	0.036/0.65	0.038/0.47	0.039/0.73	0.155/2.85	
Ours ($dlt+e2e$)	0.011/0.37	0.029/0.58	0.022/1.46	0.029/0.59	0.035/0.43	0.033/0.60	0.093/2.03	
Ours ($dlt+e2e+ref$)	0.007/0.20	0.010/0.34	0.009/0.53	0.013/0.28	0.017/0.32	0.010/0.21	0.032/0.81	
Recalls	Chess	Fire	Heads	Office	Pumpkin	Kitchen	Stairs	Avg
DSAC* [1] w/ model	99.9	98.9	99.8	98.1	99.0	97.0	92.0	97.8
Ours ($dlt+e2e$)	90.1	66.0	60.7	75.6	63.2	64.0	28.8	64.1
Ours ($dlt+e2e+ref$)	100	86.3	68.9	93.9	80.5	91.1	65.9	83.8
Ours ($dlt+e2e+dsac*$)	100	99.7	97.9	99.5	94.4	97.7	84.2	96.0

2 More ablation studies

Graph Attention Layer. As described in Section 3.2 in the main paper, we use Graph Attention Layers in the quality weight network. The quality weight network is based on OANet [8], which is a PointNet-like architecture that takes 2D-3D correspondence pairs as input. We propose to introduce the self-attention mechanism into OANet, replacing the original normalized MLP modules with Graph Attention Layers. This layer builds a fully connected graph upon clusters and conducts global message passing between all nodes. This network architecture enhancement improves the re-localization accuracy. As shown in Table 2, using the Graph Attention Layer, the median transition error for Ours (dlt) is decreased from 23cm to 18cm on *Stairs*, and 19cm to 15cm on *Shop Facade*. We also report the results of Ours ($dlt+e2e$) in Table 2, which are consistent with Ours (dlt) in most scenes.

Classification loss \mathcal{L}_c in Section 3.3 is a binary cross-entropy function which plays the role of a hard outlier pruner. It allows a more stable convergence during training, and enhances the pose estimation accuracy. \mathcal{L}_c is effective for both indoor and outdoor scenes, and especially useful for challenge environments, as shown in Table 2. For instance, it results in a relative error reduction of 77% on *Shop Facade*, whose scene coordinates are very noisy due to dynamic objects and non-Lambertian reflection.

3 Self-supervised adaptation at test time

As illustrated in the main paper, self-supervised adaptation deals with the domain shift problem during test time and significantly enhances the re-localization performance of the DLT setting. As a supplement to Fig. 4 in the main paper, we compare learned weights on Cambridge before and after self-supervised adaptation at test-time, in Fig. 1. It shows that the quality network is capable of selecting better scene coordinates after test-time adaptation.

Table 2. More ablation studies on some scenes of 7Scenes dataset [6] and Cambridge dataset [4]. We validate the effects of Graph Attention Layer and classification loss \mathcal{L}_c , and report median translational and rotational errors measured in m and $^\circ$. dlt and $e2e$ are evaluated without and with the third end-to-end fine-tuning stage mentioned in Section 3.4 of the main paper. The best results are highlighted.

		Ours (dlt)				
Attention Layer \mathcal{L}_c		Fire	Office	Stairs	Shop Facade	Church
✓		0.055/1.06	0.076/1.06	0.251/4.16	0.65/2.5	0.62/1.9
	✓	0.060/1.09	0.068/1.03	0.230/4.00	0.19/1.2	0.50/1.5
✓	✓	0.051/1.04	0.063/0.93	0.179/3.61	0.15/1.1	0.50/1.5
		Ours ($dlt + e2e$)				
	✓	0.057/1.10	0.061/ 0.84	0.163/3.06	0.12/0.7	0.35/1.3
✓	✓	0.048/1.09	0.055/0.86	0.123/2.80	0.11/0.7	0.39/1.3

Table 3. Median errors of the pose estimation on 7Scenes dataset [6] w.r.t. the self-supervised adaptation module. Translational and rotational errors are measured in cm and $^\circ$. dlt is the weighted DLT method, $e2e$, ref and $self$ denote end-to-end training step, LM-Refine and self-supervised adaptation, respectively. 150k means 150k iterations of fine-tuning. The best results are highlighted.

Methods	Chess	Fire	Heads	Office	Pumpkin	Kitchen	Stairs
Ours ($dlt+e2e+self$ [150k])	2.5/0.71	3.3/0.98	2.6/1.84	4.1/0.81	6.1/1.21	6.2/1.26	6.8/1.24
Ours ($dlt+e2e+self$ [600k])	2.1/0.64	2.3/0.80	1.3/0.79	3.7/0.76	4.8/1.06	5.1/1.08	5.5/1.48
Ours ($dlt+e2e+self+ref$ [600k])	1.9/0.62	2.4/0.86	1.3/0.69	3.4/0.76	4.9/ 1.04	5.2/1.12	4.7/1.21

In the main paper, we report the results of fine-tuning for 600k iterations on 7Scenes and Cambridge datasets. It is important to investigate how well the network adapt with fewer iterations, so as to be practical in real-world applications. As shown in Fig. 2, the median translation error of the estimated poses drops rapidly within 20k iterations (wall-clock time: 23 minutes). Thus, we show additional pose estimation results within fewer iterations (150k, wall-clock time: 2.9 hours), in Table 3 and 4. It demonstrates that the proposed self-supervised adaptation module can achieve reasonably good results using few iterations, and fine-tuning with more iterations proceeds to improve the pose estimation.

Besides, we describe the mechanism of self-supervised adaptation in detail, using Fig. 3. Specifically, we select two adjacent frames as source and target images, and warp I_s to target I_t using the predicted scene coordinates \mathbf{C}_s in

Table 4. Median errors of the pose estimation on Cambridge dataset [4] w.r.t. the self-supervised adaptation module. Translational and rotational errors are measured in m and $^\circ$. The notations are the same as Table 3. The best results are highlighted.

Methods	Greatcourt	King’s College	Shop Facade	Old Hospital	Church
Ours ($dlt+e2e+self$ [150k])	0.95/0.5	0.11/0.4	0.05/0.4	0.20/0.7	0.22/0.9
Ours ($dlt+e2e+self$ [600k])	0.94/0.5	0.11/0.3	0.05/0.4	0.18/0.7	0.17/0.8
Ours ($dlt+e2e+self+ref$ [600k])	0.28/0.2	0.08/0.2	0.04/0.3	0.11/0.4	0.09/0.3

the world coordinate system and the transform matrix \mathbf{T}_{t2w} calculated by the DLT process. Then the photometric error serves as self-supervision and back-propagates gradients along the red arrows, while others are detached in this stage. Note that the \mathbf{T}_{t2w} is post-processed by the algorithm of Section 7, which is fully differentiable and enables the gradients flowing from the photometric loss. In our experiments, the sampling interval of two images is 7 for 7-Scenes and 1 for Cambridge, respectively.

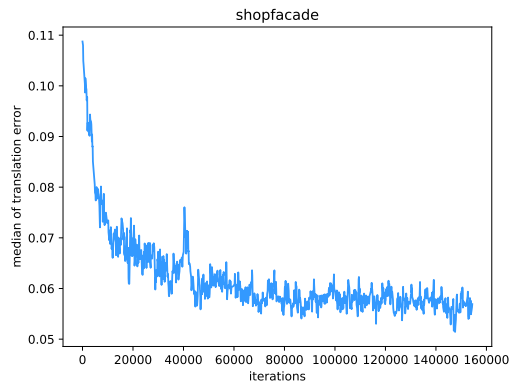


Fig. 2. The median translation error of the estimated poses on *shopfacade* (from Cambridge) during self-supervised adaptation. It rapidly converges within 20k iterations, which demonstrates the effectiveness of this module in real world scenarios.

4 3D Map visualization

In Fig. 5, we visualize point clouds predicted directly by scene coordinate regression networks and those filtered by the learned weights of our SC-wLS framework. We filter out points with weights smaller than $\lambda = 0.9$. It shows that the scene coordinates are particularly noisy and due to the nature of reprojection supervision, point clouds may drift away far along the bearing vectors. However, with the assistance of our SC-wLS, the weight-filtered point clouds are much more accurate and cleaner, showing the effectiveness and interpretability of the learned weights as well.

5 Loss functions

This section elaborates on the hyper-parameter tuning of the regression loss \mathcal{L}_r in Section 3.3. As illustrated in the main paper, we use an eigen-decomposition

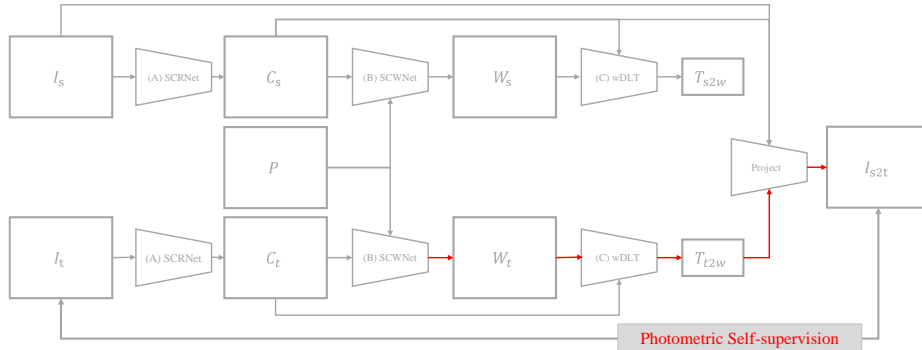


Fig. 3. A detailed illustration of the self-supervised fine-tuning procedure. I_s is the source RGB image. I_t is the target RGB image. SCRNet (A) is the scene coordinate regression network. C_s is the scene coordinate map for the source image. C_t is the scene coordinate map for the target image. P is the 2D pixel coordinate map. SCWNet (B) is the scene coordinate quality weight network. W_s is the scene coordinate weight map for the source image. W_t is the scene coordinate weight map for the target image. wDLT (C) is the weighted least squares solver. T_{s2w} is the camera pose of the source image in the world frame. T_{t2w} is the camera pose of the target image in the world frame. Only tensors that flow through red arrows receive supervision signals while others are detached.

free loss [3] to refrain from the numerical instability caused by the eigen-vector switching problem:

$$\mathcal{L}_r = \mathbf{t}^\top \mathbf{X}^\top \text{diag}(\mathbf{w}) \mathbf{X} \mathbf{t} + \alpha e^{-\beta \text{tr}(\bar{\mathbf{X}}^\top \text{diag}(\mathbf{w}) \bar{\mathbf{X}})} \quad (1)$$

where \mathbf{t} is the flattened ground-truth pose, $\bar{\mathbf{X}} = \mathbf{X}(\mathbf{I} - \mathbf{t}\mathbf{t}^\top)$, while α and β are positive scalars.

As mentioned before, those two terms in Eq. 1 serve as different roles. The former originates from $\text{diag}(\sqrt{\mathbf{w}}) \mathbf{X} \mathbf{t} = 0$, and minimizing this term leads to the trivial solution of $\mathbf{w} = \mathbf{0}$ as well. Thus the latter term is proposed to alleviate its impact. Since $\bar{\mathbf{X}}$ projects all data vectors onto the hyperplane normal to \mathbf{t} , we could maximize the trace of $\bar{\mathbf{X}}^\top \text{diag}(\mathbf{w}) \bar{\mathbf{X}}$ to make the eigenvalues corresponding to directions orthogonal to \mathbf{t} to be as large as possible. It’s important to select proper hyperparameters α and β to balance these two terms. At the same time, the magnitude of the last term varies considerably on different scenes. We recommend to choose β as the inverse of the magnitude of this trace, and in our experiments, α and β are set to 5 and $1e-4$ for indoor 7Scenes while 5 and $1e-6$ for outdoor Cambridge, respectively.

6 Network architecture

As mentioned in Section 4.1 in the main paper, we adopt the scene coordinate regression network architecture from [2] for 7Scenes. For Cambridge, we use the

same architecture as the feature encoder in RAFT [7] to replace the early layers of this network, which has residual connections, as shown in Fig 4. It increases the receptive field size of the network, and enhances the robustness of feature extraction for complicated environments. We have also tried this enhanced architecture for 7Scenes, which does not bring performance improvements.

7 Post-processing of the DLT algorithm

As described in Section 3.1 of the main paper, pose estimation is solved by the Direct Linear Transform (DLT) algorithm:

$$\mathbf{X}^\top \text{diag}(\mathbf{w}) \mathbf{X} \text{Vec}(\mathbf{T}) = 0 \quad (2)$$

where the transform matrix is flattened as $\text{Vec}(\mathbf{T})$, and corresponds to the smallest eigen-vector of $\mathbf{X}^\top \text{diag}(\mathbf{w}) \mathbf{X}$. To guarantee that the rotation matrix \mathbf{R} is orthogonal and has determinant 1, we post-process the DLT results using the common generalized Procrustes algorithm [5]. The pseudo-code of our implementation is:

Algorithm 1 Post-processing of the pose calculated by the DLT algorithm

```

1: Input:  $\bar{\mathbf{T}} = \begin{bmatrix} p_1 & p_2 & p_3 & p_4 \\ p_5 & p_6 & p_7 & p_8 \\ p_9 & p_{10} & p_{11} & p_{12} \end{bmatrix} = [\bar{\mathbf{R}}_{3 \times 3} | \bar{\mathbf{t}}_{3 \times 1}]$ , and learned weight  $\mathbf{w}$ ;
2: Output: Regularized  $\mathbf{T} = [\mathbf{R}_{3 \times 3} | \mathbf{t}_{3 \times 1}]$ ;
3:  $\mathbf{U}\Sigma\mathbf{V} = \text{SVD}(\bar{\mathbf{R}})$ ;
4:  $s = \frac{3}{\text{tr}(\Sigma)}$ ;
5: Selecting the most confident 2D-3D correspondence  $c = (u, v, x, y, z)$  according to
   the learned weight  $\mathbf{w}$ ;
6: if  $s(xp_9 + yp_{10} + zp_{11} + p_{12}) > 0$  then
7:    $s = s$ ;
8: else
9:    $s = -s$ ;
10: end if
11:  $\mathbf{R} = \text{sign}(s)\mathbf{U}\mathbf{V}^\top$ ;
12:  $\mathbf{t} = s\bar{\mathbf{t}}$ ;

```

It’s worth noting that these steps are fully differentiable, thus the self-supervised adaptation in Section 3.6 is able to back-propagate gradients through this operation.

8 Error Metrics

Median errors are robust to outlier estimates. We report the translation and rotation errors per testing frame on *office* and *kingscollege* in Fig. 6. It’s shown

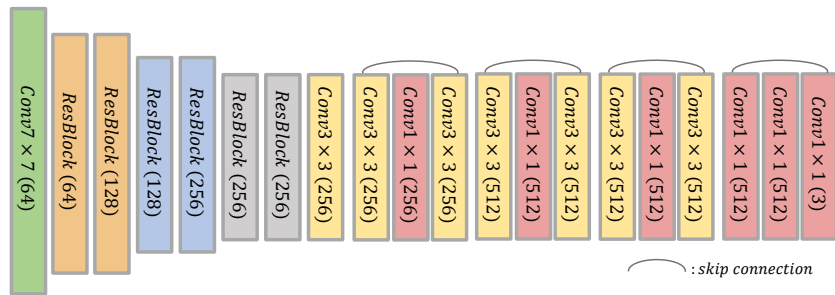


Fig. 4. Scene coordinate regression network details for Cambridge. The first 8 blocks are the same as the feature encoder in [7], and no normalization is used. Skip connections are used in both ResBlocks and the last 12 blocks as denoted.

that per frame error may be negatively impacted by outliers thus hard to tell the true algorithm performances, while median errors are easier to compare between lots of methods. We have released the code for per frame error analysis.

9 Delving into Interpretability

As for interpretability, we report pearson correlation coefficients between learned weights and inverse reprojection errors in Table 5, in which outdoor scenes give higher correlation values due to many uncertain regions like sky and human.

Table 5. Pearson correlation coefficients. ($p < 0.01$)

Chess	Fire	Heads	Office	Pumpkin	Kitchen
0.18	0.15	0.18	0.15	0.21	0.14
Stairs	Court	College	Shop	Hospital	Church
0.21	0.23	0.22	0.23	0.24	0.21

References

1. Brachmann, E., Humenberger, M., Rother, C., Sattler, T.: On the limits of pseudo ground truth in visual camera re-localisation. In: Proceedings of the IEEE/CVF International Conference on Computer Vision. pp. 6218–6228 (2021) 1, 2
2. Brachmann, E., Rother, C.: Visual camera re-localization from rgb and rgb-d images using dsac. IEEE Transactions on Pattern Analysis and Machine Intelligence (2021) 5
3. Dang, Z., Yi, K.M., Hu, Y., Wang, F., Fua, P., Salzmann, M.: Eigendecomposition-free training of deep networks for linear least-square problems. TPAMI (2020) 5

4. Kendall, A., Grimes, M., Cipolla, R.: PoseNet: A convolutional network for real-time 6-dof camera relocalization. In: ICCV (2015) [3](#)
5. Schönemann, P.H.: A generalized solution of the orthogonal procrustes problem. *Psychometrika* **31**(1), 1–10 (1966) [6](#)
6. Shotton, J., Glocker, B., Zach, C., Izadi, S., Criminisi, A., Fitzgibbon, A.: Scene coordinate regression forests for camera relocalization in rgb-d images. In: CVPR (2013) [2](#), [3](#)
7. Teed, Z., Deng, J.: Raft: Recurrent all-pairs field transforms for optical flow. In: European conference on computer vision. pp. 402–419. Springer (2020) [6](#), [7](#)
8. Zhang, J., Sun, D., Luo, Z., Yao, A., Zhou, L., Shen, T., Chen, Y., Quan, L., Liao, H.: Learning two-view correspondences and geometry using order-aware network. In: ICCV (2019) [2](#)

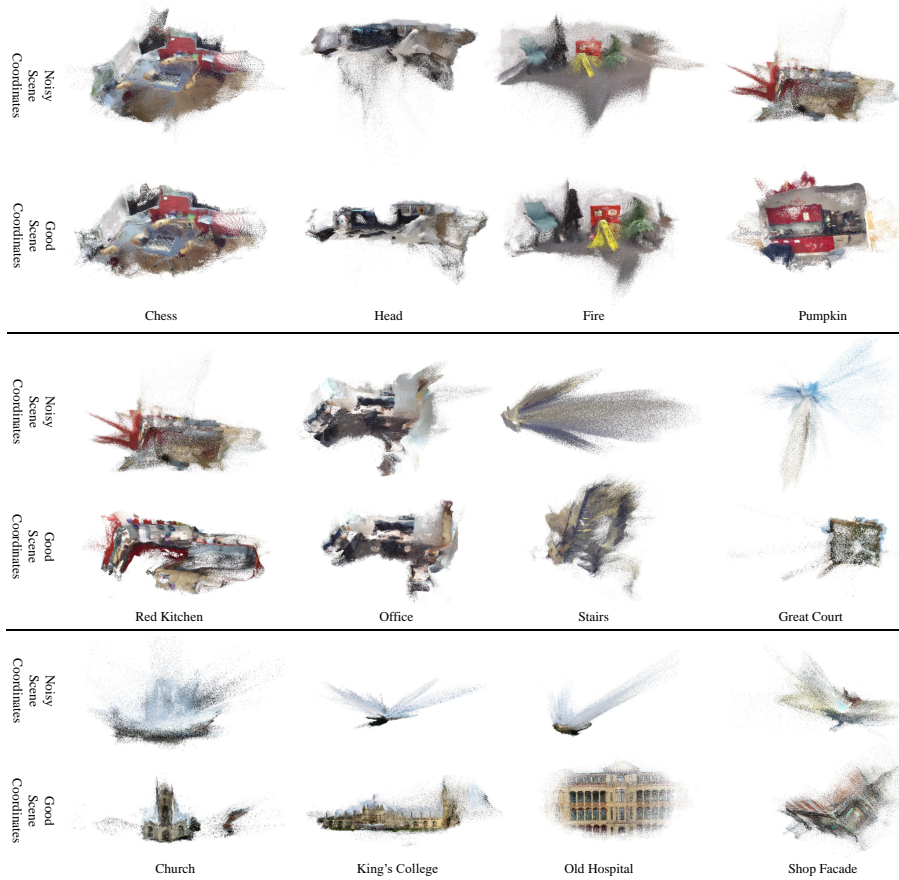


Fig. 5. Map visualization on the test sets of 7-Scenes and Cambridge. Since scene coordinates are predicted in the world frame, we directly show the point clouds generated by aggregating scene coordinate predictions on test frames. It can be seen that only predicting scene coordinates results in noisy point clouds, especially in outdoor scenes where scene coordinate predictions on sky regions are only meaningful in term of their 2D projections. We show good scene coordinates by filtering out samples with a quality weight lower than 0.9.

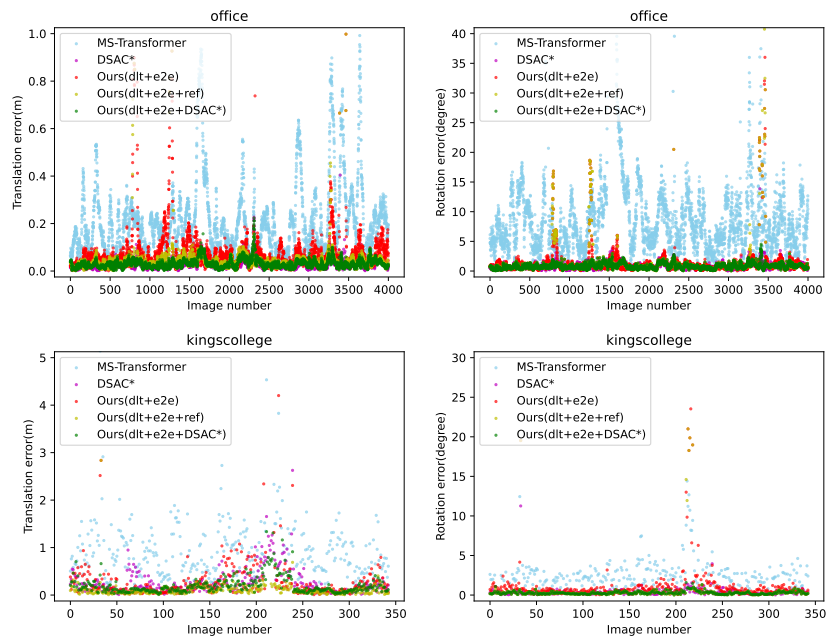


Fig. 6. Translation and rotation errors per testing frame.